Natural Resources Research (© 2022)
https://doi.org/10.1007/s11053-022-10064-5

Original Paper

Constraints on the Geometry and Gold Distribution in the Black Reef Formation of South Africa Using 3D Reflection Seismic Data and Micro-X-ray Computed Tomography

Glen T. Nwaila,[1,8] Musa S. D. Manzi,[1] Steven E. Zhang,[2,3] Julie E. Bourdeau,[3] Lunga C. Bam,[4] Derek H. Rose,[5] Kebone Maselela,[1] David L. Reid,[6] Yousef Ghorbani,[7] and Raymond J. Durrheim[1]

Received 6 November 2021; accepted 27 March 2022

Geological and geophysical models are essential for developing reliable mine designs and mineral processing flowsheets. For mineral resource assessment, mine planning, and mineral processing, a deeper understanding of the orebody's features, geology, mineralogy, and variability is required. We investigated the gold-bearing Black Reef Formation in the West Rand and Carletonville goldfields of South Africa using approaches that are components of a transitional framework toward fully digitized mining: (1) high-resolution 3D reflection seismic data to model the orebody; (2) petrography to characterize Au and associated ore constituents (e.g., pyrite); and (3) 3D micro-X-ray computed tomography (μCT) and machine learning to determine mineral association and composition. Reflection seismic reveals that the Black Reef Formation is a planar horizon that dips < 10° and has a well-preserved and uneven paleotopography. Several large-scale faults and dikes (most dipping between 65° and 90°) crosscut the Black Reef Formation. Petrography reveals that gold is commonly associated with pyrite, implying that μCT can be used to assess gold grades using pyrite as a proxy. Moreover, we demonstrate that machine learning can be used to discriminate between pyrite and gold based on physical characteristics. The approaches in this study are intended to supplement rather than replace traditional methodologies. In this study, we demonstrated that they permit novel integration of micro-scale observations into macro-scale modeling, thus permitting better orebody assessment for exploration, resource estimation, mining, and metallurgical purposes. We envision that such integrated approaches will become a key component of future geometallurgical frameworks.

KEY WORDS: Gold, South Africa, 3D seismics, Machine learning, 3D micro-X-ray computed tomography.

[1]Wits Mining Institute (WMI) and School of Geosciences, University of the Witwatersrand, 1 Jan Smuts Ave., Johannesburg 2000, South Africa.
[2]PG Techno Wox (Pty) Limited, 39 Kiewiet Street, Helikon Park 1759, South Africa.
[3]Geological Survey of Canada, 601 Booth Street, Ottawa, ON K1A 0E9, Canada.
[4]Department of Radiation Science, Nuclear Energy Corporation of South African (NECSA), Pretoria 0001, South Africa.
[5]Department of Geology, University of Johannesburg, P.O. Box 524 Auckland Park 2006, Gauteng, South Africa.
[6]Department of Geological Sciences, University of Cape Town, Rondebosch 7700, South Africa.
[7]Department of Civil, Environmental and Natural Resources Engineering, Luleå University of Technology, SE–971 87, Luleå, Sweden.
[8]To whom correspondence should be addressed; e-mail: glen.nwaila@wits.ac.za

Published online: 28 April 2022

INTRODUCTION

Historically, Witwatersrand-type gold deposits of South Africa ranked at the pinnacle of world gold production (Hartnady, 2009; Frimmel, 2019). In 1970, South Africa produced roughly 1000 metric tons of gold (Frimmel & Nwaila, 2020). This amount has steadily decreased over the years to only about 82 metric tons in 2021 (USGS, 2021). Nonetheless, there may be potential for sustaining and perhaps even increasing future production, thereby contributing to South Africa's economic prosperity. The Witwatersrand-type 'mega-deposits' are the result of spectacularly fortuitous preservation of a significant proportion of gold that was recycled into cratonic sedimentary basins of that age (Robb & Robb, 1998; Frimmel, 2005) and skew models of the crustal gold endowment to an early period in Earth's history (Frimmel, 2014).

Most active mines that extract gold from the Witwatersrand Basin suffer from high operational costs linked to the ever-increasing depths of the remaining resources, structural complexities or erratic deposit (also called 'reef') distribution at shallower depths (Frimmel & Nwaila, 2020). Although perennial issues of fluctuating metal prices, marginal ore grades, uncertainties in global supply and demand, capital expenditure, workforce skills, sociopolitical ideologies, environmental degradation, and investment incentives affect the entire South African mining industry, the relatively high production cost of gold from the Witwatersrand Basin remains to be addressed adequately. Cost reductions are required throughout the resource extraction process, whether through reduced expenditures or increased operational efficiency. In the exploration and mining industry, the assay of gold in ore samples presents unique challenges, compounded by complex and multiscale natural distribution patterns (e.g., lognormality, nugget effect), all of which influence strongly data replicability, accuracy and predictability of any resource being assessed. Questions concerning where, how and what to sample, coupled with strategic decisions about why and when, all demand utmost diligence and dedication (Minnitt, 2014). Even the most ''perfect'' sample suite can be limited by problems unique to laboratory analytical procedures (e.g., fire assay) required to determine accurately and precisely gold contents, especially under time and money constraints that pervade the industry (Williams, 2020). Improvements upon the traditional assay process could conceivably come from machine learning and data repurposing.

The century-long mining history of Witwatersrand-type ore has produced a legacy of readily available datasets about (1) resource location, (2) resource estimation and (3) resource extraction, all of which can be used for 3D visualization and data-driven analytics (Ghorbani et al., 2020; Nwaila, et al., 2020c; Zhang et al., 2021). These latter published studies have targeted ore deposits hosted by the Central Rand Group of the Witwatersrand Basin. These legacy datasets provide a natural dry laboratory to test geological hypotheses, as well as 'ground truth' that is necessary to evaluate quantitative models. In contrast, this study focused on the geologically younger (Neoarchean to Paleoproterozoic) Black Reef Formation in the West Rand and Carletonville goldfields (South Africa). Despite being discovered in the 1880s, the Black Reef Formation remains the least explored and exploited gold-bearing formation in South Africa. In this study, we used seismic attributes, and 3D micro-X-ray computed tomography (μCT) data to explore the subsurface distribution of the Black Reef Formation and its associated geological structures. We demonstrate that such information can be used in an integrated manner to perform rapid resource assessment, which may improve grade control and resource estimation models.

GEOLOGICAL SETTING

Witwatersrand-type gold deposits and associated lithologies occur within the central portion of South Africa (Fig. 1). Four significant periods of Witwatersrand-type gold deposition have been recognized, spanning roughly 500 My. The oldest is the Dominion Reef Group, followed by the Witwatersrand Supergroup (West Rand and Central Rand Groups), the Ventersdorp Supergroup (Ventersdorp contact reef) and finally, the Transvaal Supergroup (Black Reef Formation). In certain parts of the Witwatersrand Basin (e.g., West Rand, Carletonville and Klerksdorp goldfields), these three stratigraphic sequences are vertically stacked (e.g., 5000–7000 m of combined thickness) and have been exploited simultaneously depending on grade or mining strategy (Fig. 2). Historical reports of gold in the Black Reef Formation in 1885 (Penning, 1891) may have just preceded the proclamation of those in the Witwatersrand Basin in 1886 (Antrobus et al., 1986).

Constraints on the Geometry and Gold Distribution

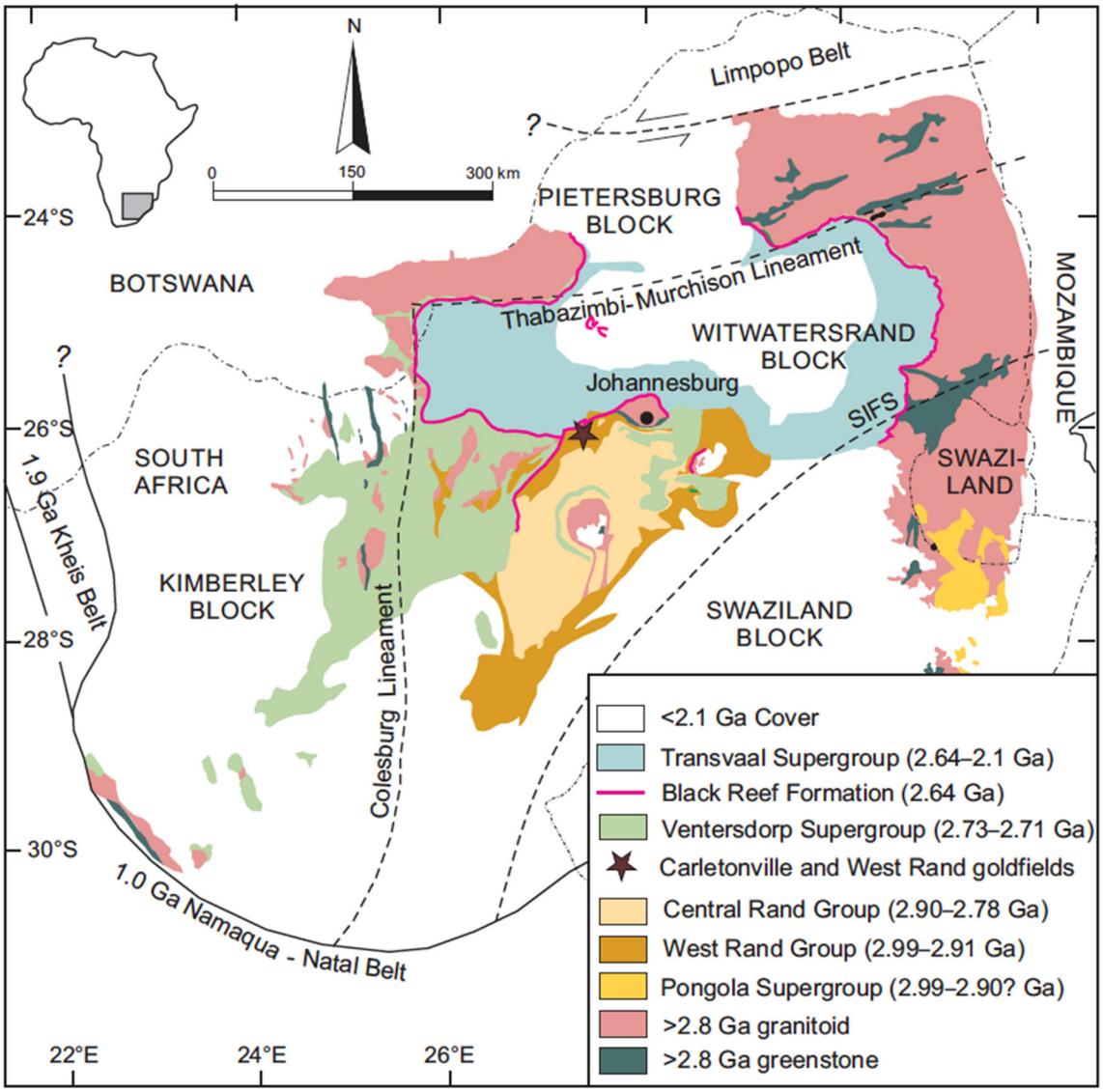

Figure 1. Simplified geological map of the Kaapvaal Craton in southern Africa showing the distribution of the three great basins (Witwatersrand, Ventersdorp and Transvaal) that host Witwatersrand-type gold deposits (modified after Frimmel, 2014). The outline of the Black Reef Formation is shown by the pink line rimming the Transvaal Supergroup.

Gold in the higher grade Ventersdorp contact reef and Central Rand Group was mined preferentially since their discovery, often to great depths. However, gold in the Black Reef Formation was only mined at the surface or near-surface, leaving deeper resources unexploited. Mounting problems of ultra-deep mining has led to a renewed focus on shallower, albeit lower-grade resources.

The Black Reef Formation occurs at the base of the 2.65–2.05 Ga Neoarchean–Paleoproterozoic Transvaal Supergroup (Transvaal Basin) and overlies an erosion surface developed on the older Witwatersrand and Ventersdorp strata in the Witwatersrand goldfields area (Els et al., 1995; Fig. 2). Elsewhere, the Transvaal Supergroup sequences overstep onto an older Archean granite-greenstone basement (Fig. 1), where isolated lenses of a pre-Black Reef Formation protobasinal clastic sequences, the Wolkberg and Gondwana Groups, are preserved (Button, 1973; Eriksson et al., 2006). Succeeding the Black Reef Formation are shallow marine carbonates and iron formations (Chuniespoort Group), followed by another largely clastic sequence (Pretoria Group). The Black Reef

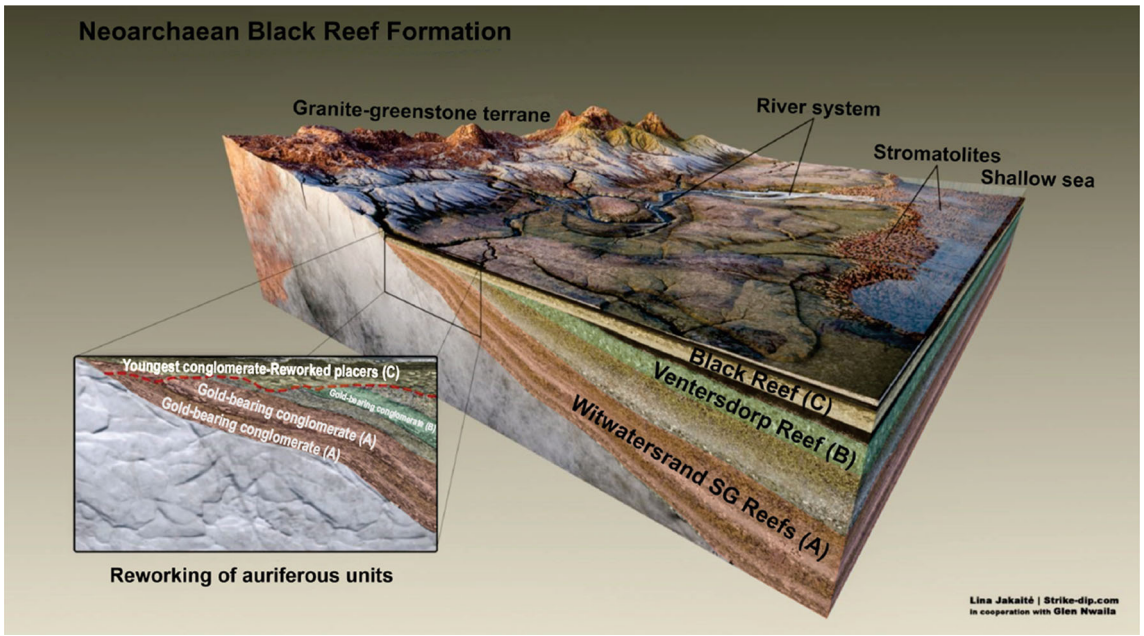

Figure 2. Reconstruction of South African Witwatersrand-type gold deposits (Nwaila et al., 2020a). Periodic reworking of the alluvial fans led to three distinct stratigraphic horizons (also referred to as 'reefs') of gold concentration. Here, A = Witwatersrand Supergroup reefs (2902 Ma), B = Ventersdorp reef (2785 Ma) and C = Black Reef Formation (2640 Ma). Scale approximation: 350 km long, 200 km wide, and each orebody (reef) horizon is 0.2 to 2 m.

Formation resembles Witwatersrand-type gold deposits in terms of economic concentration of its gold, mineralogy and depositional environment (Barton & Hallbauer, 1996; Fuchs et al., 2016).

Detrital zircon U–Pb dates support a maximum depositional age of 2618 ± 11 Ma (Zeh et al., 2020) for the Black Reef Formation, which is composed of massive to cross-bedded, weakly metamorphosed quartz arenites, clay- and siltstones, carbon-rich shales, and small conglomerates with variable auriferous deposits. Economic gold concentrations are found in the East Rand, Carletonville and West Rand goldfields where N–S trending paleochannels deeply eroded the underlying auriferous Ventersdorp and Witwatersrand strata (Barton & Hallbauer, 1996). There, grades can reach 54.5 g/t gold and 600 g/t uranium. Elsewhere, concentrations are low (< 1 g/t Au and 10 g/t U; Fuchs et al., 2016), and thus far, limited gold has been found in locations where the Black Reef Formation overlies Wolkberg protobasin clastics or Archean granite-greenstone basement (Fig. 1).

Three distinct Black Reef facies are found in the East Rand, namely the (progressing up-section): (1) channel facies, which may be locally absent and is variably gold-bearing; (2) blanket facies—a basal unit that is widespread and poorly mineralized; and (3) pyritic facies—a pyrite-bearing unit that is typically well-mineralized (Henry & Master, 2008; Fuchs et al., 2016). Similar facies were recognized by Nwaila et al. (2020a, 2020b) in the Carletonville goldfield. The gold-bearing quartz-pebble conglomerates of the Black Reef Formation are dominantly composed of quartz, pyrite, phengitic white mica, clay minerals, carbonates, chromite, zircon, rutile, pyrrhotite, sphalerite, galena, uraninite and native gold (Fuchs, 2015). As with all other gold-bearing conglomerates found in the Witwatersrand Basin, pyrite, the most abundant ore mineral in the Black Reef ore deposit, can be classified into three main classes (da Costa et al., 2020): (1) detrital (or allogenic) pyrite; (2) diagenetic (or authigenic) pyrite that formed in situ after deposition; and (3) hydrothermal (or epigenetic) pyrite related to post-depositional alteration. Detrital pyrite appears rounded and can be massive or inclusion-bearing (< 10 vol % of Au, Ag, Ni, and other metals). Isotopic analyses ($\delta^{34}S$ and $\delta^{33}S$) of detrital pyrite reveal contrasting formation processes and thus different provenances for detrital pyrite (Hofmann et al., 2009; Guy et al., 2014; Agangi et al., 2015; da Costa et al., 2020). Authigenic pyrite is characteris-

tically large and subhedral, while hydrothermal pyrite is euhedral to subhedral in shape. Most pyrite grains are massive, although some contain gold and other metals (Hofmann et al., 2009; Agangi et al., 2015). Most authigenic pyrite grains formed after sedimentation, diagenetic, hydrothermal or metamorphic processes (da Costa et al., 2020). Gold in the Black Reef Formation occurs either as isolated native grains or inclusions in pyrite and pyrobitumen nodules (Fuchs et al., 2016). In certain areas, gold is found within fractured quartz grains and, to a lesser degree, in adjacent footwall lithology.

SAMPLES AND METHODS

3D Reflection Seismic Post-Processing and Extraction of Point Cloud

Modeling of the structurally complex Black Reef Formation involved: (1) 3D seismic imaging; (2) identification of the horizon and faults in 3D (inline, crossline and depth slices); (3) data filtering; (4) evaluation of seismic data using seismic attributes to enhance geological structures; (5) fault-horizon projection; and (6) 3D seismic data integration with borehole.

The seismic data were first processed to remove spikes/outliers. Next, the Black Reef Formation horizon and associated geological structures (i.e., faults and dikes) were identified and tracked in 3D. Artefacts were smoothed using various filters, including the bi-harmonic smoothing technique to enhance structural interpretation. The edge detection attribute analysis improved fault-horizon projection (Manzi et al., 2012a, 2012b). Using these techniques, faults and dikes could be identified and located with maximum accuracy, and errors associated with false complex geometries are minimized. The point clouds generated from the fault-horizon network were then used to model fault surfaces, resulting in close correlations with the seismically defined Black Reef Formation horizon breaks. The point cloud for the entire seismic volume consists of > 1 million data points.

Samples

The study area lies between 26° 25′ 46'' S, 27° 37′ 20'' E and 26° 21′ 29'' S, 27° 23′ 53'' E, encompassing the West Rand and Carletonville goldfields (Fig. 1). A portion of the data for this study originated from a legacy database, which contains 23 borehole lithologic logs. Samples from the lithologic logs were scanned using micro-X-ray computed tomography (μCT). The lithologic logs consist of sample descriptions and spatial positions (latitude, longitude and depth). Where necessary, the historical boreholes were re-logged to ensure consistency of data recording.

In addition to the legacy database, five boreholes were drilled and sampled between 2015 and 2020. To improve the classification of pyrite and gold morphology, 100 samples from the five boreholes (20 samples per borehole) were separated into mineral grains. Care was taken to prepare coarsely crushed samples > 1 mm to avoid destroying pyrite grains. The usable fraction (> 500 μm) was first separated using manual panning. Both dense and light particles were separated and washed with acetone and deionized water, and subsequently placed in an oven to dry. Further, pyrite concentration utilized bromoform with a density of 2.89 g/cm^2. Stirring of the high-density grain fraction released finer, less dense grains entrained during initial separation in the bromoform. The cleaned grain separate was collected from the funnel onto filter paper, washed in acetone, then deionized water, and then left to dry overnight in a fume hood. A magnet was used to separate ferromagnetic minerals and any iron filings that may have been introduced during crushing and milling, followed by a rare earth element magnet to separate paramagnetic minerals. The remaining material underwent further separation of pyrite using a Frantz Isodynamic Magnetic Separator set with a 25° forward slope, a 10° sideways tilt and 1.2A current. Final handpicking enabled visual classification of pyrite grains into three different morphologies—detrital, diagenetic and hydrothermal.

X-Ray Computed Tomography (μCT)

Most automated mineralogical tools currently used are based on two-dimensional (2D) microscopy analysis, bound by stereological error when analyzing a three-dimensional (3D) object such as ore particles. The latest advancements in μCT have shown the great potential of such a system to be the following automated mineralogical tool (Ketcham, 2005; Kyle & Ketcham, 2015; Hanna & Ketcham, 2017; Withers et al., 2021; da Costa et al., 2022). An

essential benefit of μCT lies in its capability to map the 3D internal structure of the ore at resolutions down to the technique's resolution limit—a few microns, for removing stereological errors (Kyle et al., 2008; Ketcham & Hildebrandt, 2014; Ketcham & Mote, 2019). Due to the constant improvement in the computing capacity of large datasets, μCT systems have become a popular tool for automated quantitative mineralogical characterization (Ghorbani et al., 2011; Evans et al., 2015; Sayab et al., 2016; Guntoro et al., 2019a, 2019b; 2020, 2021; Warlo et al., 2021). This study evaluated the applicability of μCT (using its typical processed output) as a tool for ore characterization. Specifically, data used in this study were obtained from auriferous conglomerates and a subset of pyrite and gold grains. High-quality images were obtained by scanning the samples at 130 kV, 51 μA, yielding 2000 projections at 4–8 μm resolution. The X-ray instrument used to acquire the data was the Nikon XTH 225 ST system situated at the MIXRAD facility at NECSA (South African Nuclear Energy Corporation; Hofmann, 2012). The sample information or parameters were obtained using VG Studio Max 3.4.0 version.

RESULTS

Resource Location Using 3D Reflection Seismics

The Black Reef Formation is one of the few remaining Witwatersrand-type gold resources located at shallow depths (< 300 m below surface). Exploration by surface borehole drilling has so far provided limited inferred resources, but, although wide gaps in the subsurface record still exist, there has been little incentive to follow-up. Only after 3D reflection seismic surveys were carried out between the 1980s and 2000s did the opportunity arise to delineate the extent of the Black Reef Formation in the West Rand and Carletonville goldfields, including areas missed by earlier drilling and mining.

The re-processed and re-interpreted legacy 3D seismic survey data demonstrate that quartzites and conglomerates of the Black Reef Formation produce a prominent and laterally extensive acoustic impedance contrast between the overlying dolomites of the Chuniespoort Group (roughly 6700 m/s seismic velocities [Vp] and 3.00 g/cm^3 density) and the underlying lower-velocity, less dense Ventersdorp meta-basalts (roughly 6400 m/s seismic velocities [Vp] and 2.90 g/cm^3 density; Manzi et al., 2013, 2014). This acoustic impedance contrast gives strong reflections within the seismic volume (Fig. 3). The edge detection (Fig. 3a) and dip-azimuth (Fig. 3b) attributes computed for the Black Reef Formation horizon suggest that the formation is characterized by a series of steeply dipping (65°–90°) complex normal faults and dikes.

In addition to revealing Black Reef Formation in 3D, the seismic data also assisted in assembling and assessing structural information pertinent to mining. Mining is severely affected by fault distribution patterns, position, continuity, strike, dip, dip direction, pitch and hade, fault length, fault spacing (compartmentalization), fault offset (throws) and fault heave. The complexity of faults and dikes can be evaluated by using seismic attributes to reveal: (1) multiple segments that bind discrete orebody blocks; (2) multiple bifurcations from a single plane to form a branching fault/dike array; and (3) cross-cutting fault/dike systems, which may be offset by older faults (Fig. 3b). In order to arrive at an accurate assessment of the orebody's financial value, mine design and life of mine planning, fault/dike arrays, and sections of the mine that may be considered risky for fault/dikes are crucial (Stevenson et al., 2003; Manzi et al., 2014). Several faults and dikes are present in the formation horizon, which may influence mining and misrepresent the distribution of gold ore within the horizon. We evaluated the effect on mining that faults and dikes could have on the horizon. The latest modeling techniques make it easier to create models that can incorporate the complexity of structural architectures, therefore optimizing evaluations of ore resources and production rates. An improved gold resource model and potential geohazards such as water conduits, seismic zones, and planes of weakness are provided. Mining-induced seismic events, rock falls, rock bursts and other hazards can be mitigated by using a horizon/deposit-scale model to identify lateral and vertical heterogeneities that require attention during mine planning (Stevenson et al., 2003). It is worth noting that the Black Reef Formation lies above several auriferous conglomerates horizons of the Ventersdorp and Witwatersrand Supergroups (Fig. 4). The model in Figure 4 shows that some of the geological structures (as gaps in horizon planes) that affect the

Constraints on the Geometry and Gold Distribution

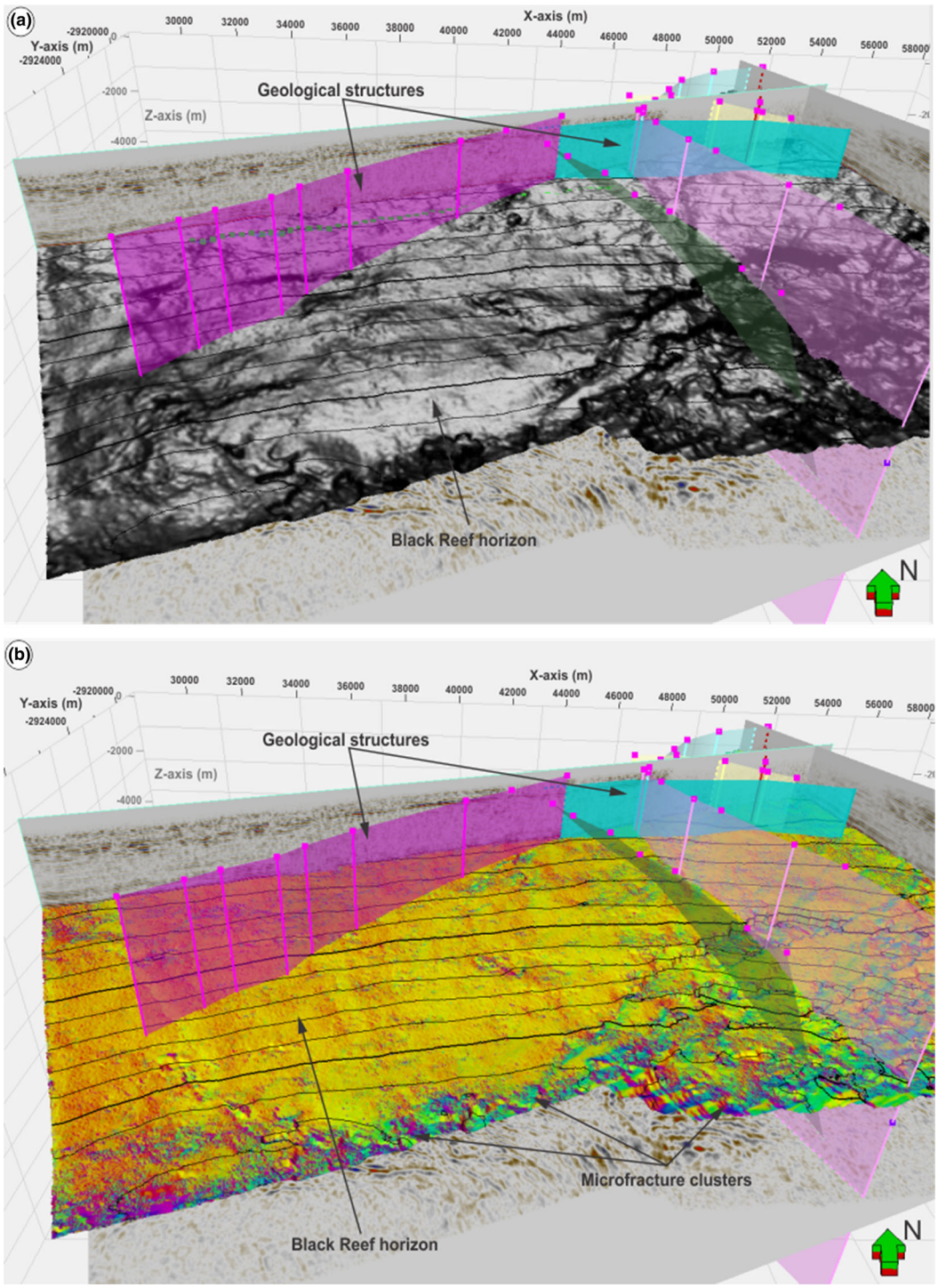

Figure 3. 3D seismic reflection cube of the Black Reef Formation horizon showing geological structures. Normal faults are depicted as purple surfaces and dikes as green surfaces. (**a**) The edge detection seismic attribute grayscale horizon delineates major geological structures. (**b**) Color depiction using the dip-azimuth seismic attribute enhances subtle geological structures.

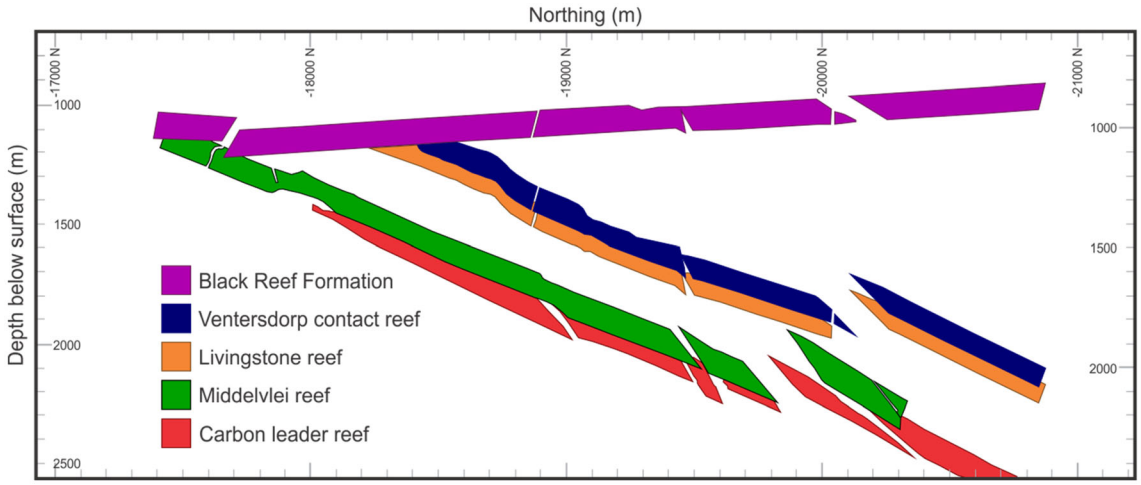

Figure 4. 3D model of gold-bearing horizons (as planes) in the Carletonville goldfield. The easting axis is nearly perpendicular to the page. Ventersdorp contact reef belongs to the Ventersdorp Supergroup; the Livingstone Reef, Middelvlei Reef and Carbon Leader Reef belong to the Witwatersrand Supergroup. The average thickness of each planar horizon is 43 cm.

Black Reef Formation can be traced downward into the underlying older auriferous horizons.

Resource Assessment

Petrographic studies target mineral assemblages and textural domains that may serve as proxies for gold distribution, thereby offering an initial screen to reduce (or even remove) the need for expensive, time-consuming laboratory fire assays. This mineralogical and textural approach could provide a means to smoothen the extreme variability in gold grain size and spatial distribution. In particular, we focus on the association between nano- to micron-scale gold grains and their host gangue minerals, which in turn occurs in textural domains at the dm to m scale.

Petrographic Characterization of Pyrite Grains

The Black Reef Formation is characterized by quartz-pebble conglomerates of varying thickness. The footwall is quartz-arenite whereas the hanging wall is carbonaceous shale (Fuchs et al., 2016; Nwaila et al., 2020a, 2020c). Minerals present in minor or trace amounts but of significant interest in the Black Reef Formation include pyrite, chromite, zircon, rutile, chalcopyrite, arsenopyrite, gersdorffite, cobaltite, pyrrhotite, galena, sphalerite, uraninite, brannerite, monazite and xenotime (Fig. 5; Fuchs et al., 2016). Gold occurs as electrum with 5–15% Ag (Gauert et al., 2011; McLoughlin, 2014). Uraninite is associated with pyrobitumen.

Detrital pyrite is the most abundant mineral found in minor amounts within the Black Reef Formation, with grains being commonly sub-rounded to rounded with abraded edges and very few (< 5 vol %) inclusions of chalcopyrite or pyrrhotite (Fig. 6; Fuchs, 2015; Fuchs et al., 2016; da Costa et al., 2020). Diagenetic pyrite grains are large (0.5–10 mm) and appear rounded, concretionary and highly porous (> 10 vol %). The morphology of diagenetic grains varies from being relatively compact and massive, some with internal lamellar structures (i.e., pyrite sand-dollar), to highly porous. Pores can be filled with muscovite, quartz, and pyrobitumen, with numerous inclusions of sphalerite, chalcopyrite and native gold. Hydrothermal pyrite occurs either as individual euhedral to subhedral inclusion-free grains or as narrow overgrowths (< 15 μm) on pre-existing pyrite.

Mineralogical Characterization Using μCT

Grains are distinguishable by their linear attenuation coefficients under X-ray radiation. Attenuation coefficients are determined by the

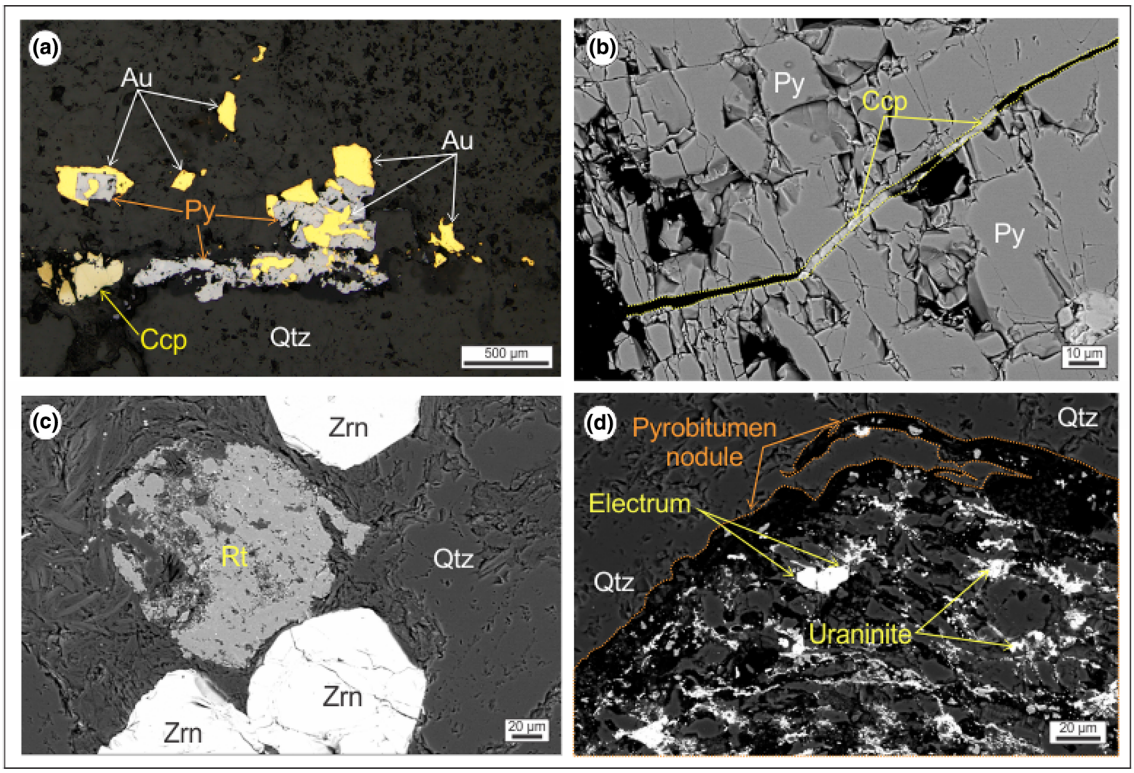

Figure 5. (**a**) Microphotographs of the Black Reef Formation gold ore in reflected light. (**b–d**) SEM images. Py = pyrite, Ccp = chalcopyrite, Rt = rutile, Zrn = zircon and Qtz = quartz.

average atomic number of chemical elements within minerals (Ghorbani et al., 2011; Guntoro, et al., 2019a; Bam et al., 2020). Witwatersrand gold-bearing ores are particularly conducive to analytical segmentation due to the high attenuation contrast of gold (very high), pyrite (medium) and quartz (low). Scanning solid ore specimens and reconstruction into a 3D digital volume (computed tomography) renders the sample available for visual analysis and quantitative measurement at the micron scale (µCT). Gold, electrum, pyrite and silicates are easily segmented based on their attenuation coefficients, while other minerals such as rutile, uraninite, and zircon tend to have impurities that preclude them from being isolated unless the scanning parameters are calibrated to identify them. In our case, the identification of phases that overlap significantly in terms of their attenuation coefficients was performed using SEM imaging as shown in Figure 5b–d.

To demonstrate the importance of µCT, a select suite of pyrite grains from the Black Reef Formation was investigated. The operating conditions of the CT scanner were such that the resolution of the volume was 4.6 µm; consequently, natural grains smaller than this voxel size (voxel = 3D pixel) cannot be unambiguously distinguished. In practice, this voxel size limitation dictates the smallest resolvable gold grain and the definition of grain boundaries between minerals of differing attenuation, but 4.6 µm is a practical optimization of analysis time and accurate gold detection. The distinct gray values between gold and associated minerals result in clear grain boundaries (Figure 7a), which can be enhanced by assigning a false color to the respective gray ranges for pyrite and gold (Figures 7b, c, d). The relationship between gold and other minerals such as pyrite is visualized and quantified in Figure 7c. It is clear that gold occurs as either free native grains or enclosed in pyrite. Figure 7b shows the distribution of gold grains which permits textural and size quantification. The dataset acquired in Figure 7b was used to plot a gold and uraninite distribution curve in Figure 8. Grain size distributions curves are an essential factor for all mineral processing stages.

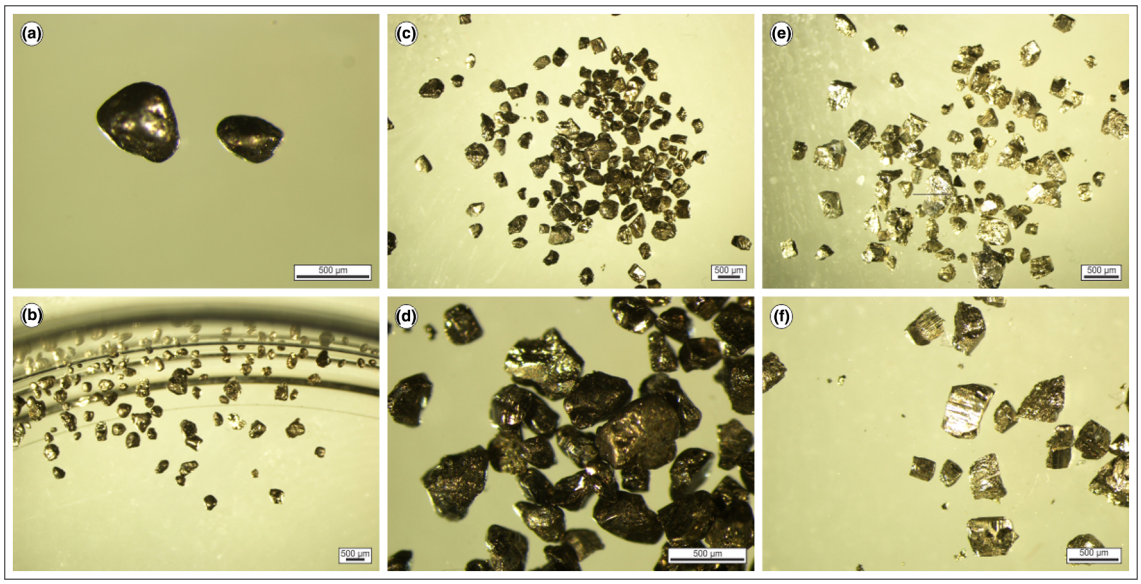

Figure 6. Petrographic classification of pyrite grains liberated from their host rock by selective acid leaching. (**a**, **b**) contain rounded detrital pyrite. (**c**, **d**) contain sub-rounded diagenetic pyrites—these pyrite grains still show crystal shapes but with slightly rounded corners/edges. (**e**, **f**) contain hydrothermal crystalline pyrite with sharp corners and striations.

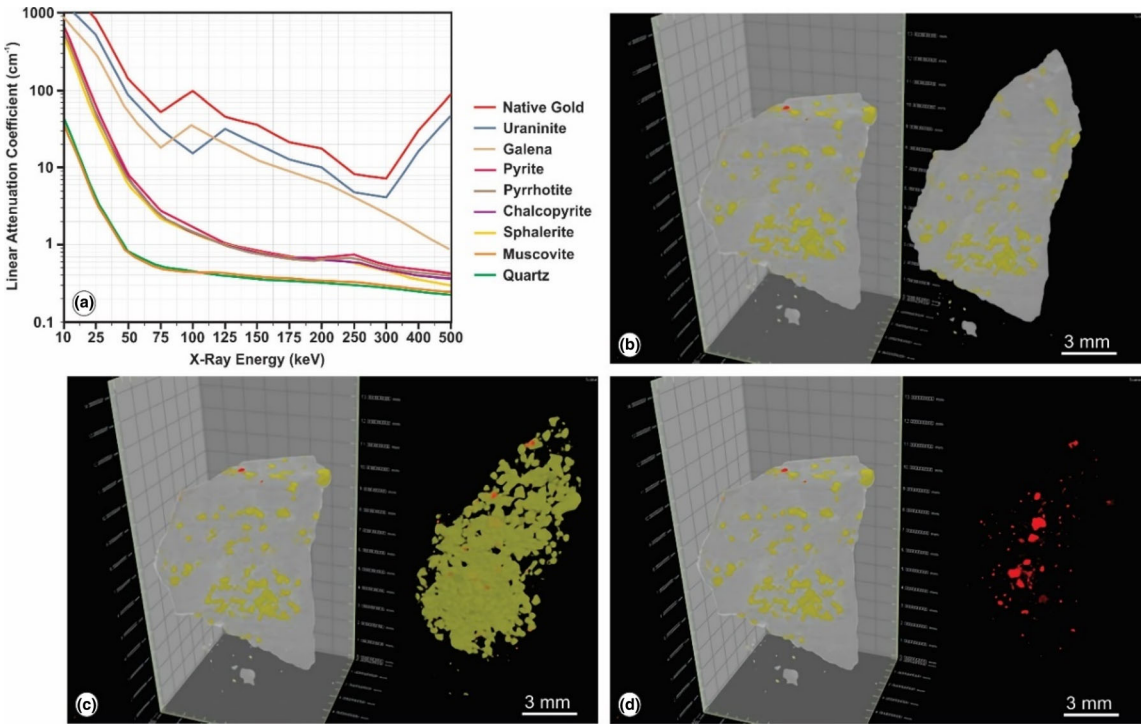

Figure 7. 3D µCT reconstruction of auriferous conglomerate from the Black Reef Formation. (**a**) X-ray attenuation coefficients over a range of scanning energy spectrum to optimize mineral identification. (**b**–**d**) Sequential artificial color segmentation to better visualize pyrite (yellow), gold (red) and other gangue minerals (gray). The attenuation data values shown here are based on end-member compositions and densities and were calculated using the MuCalc (Hanna & Ketcham, 2017).

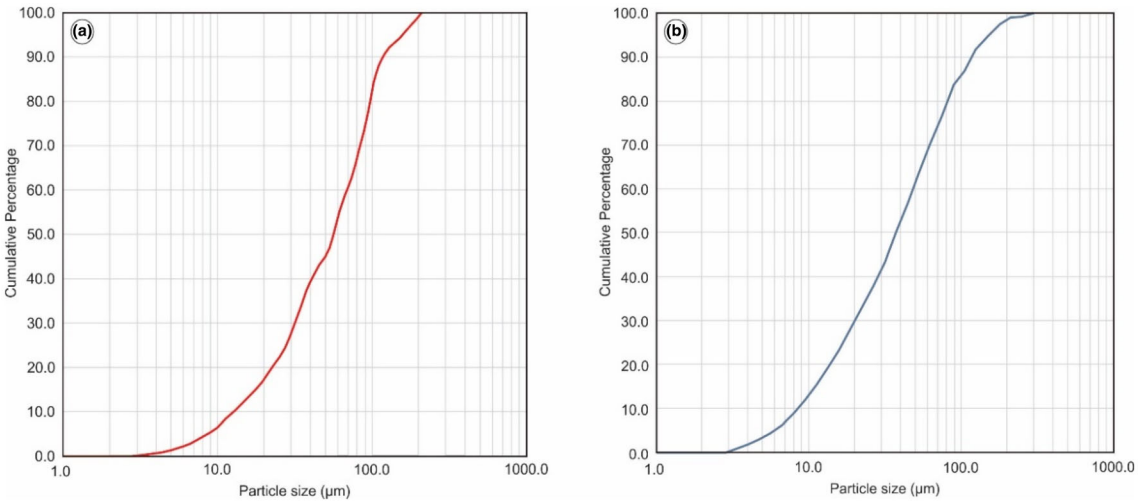

Figure 8. 3D Grain size distribution indicating the variation of the (**a**) gold grain sizes and (**b**) uraninite grain sizes in the Black Reef Formation.

Machine Learning Characterization of Gold and Pyrite from μCT Data

Machine learning as a sub-discipline of artificial intelligence is concerned with the ability of machines to leverage algorithms to perform deductive and inductive reasoning, often in an automated manner. Like humans, machine learning algorithms allow a machine to perform various deductive tasks, such as classifying and modeling natural relationships in the data through training. Once a machine learning algorithm is trained, it can perform classification and regression tasks through inductive reasoning. Therefore, it is possible to use machine learning to discriminate between gold and pyrite and among various types of pyrite using μCT data (Figs. 7 and 9). This study made use of μCT data from whole-rock samples. A quality control was performed by assessing the validity of the results with individual pyrite and gold grains as described in the previous section and verified by SEM imaging results in Figure 5.

Spatial calibration of the 3D volume allows quantitative dimensional measurements to be made, from which many useful textural properties (albeit within individual grains) can be derived. Grain analyses in the search for internal structure and relationships with enclosed gold particles led to the creation of a comprehensive spatial characteristics database, which also contains relative particle X-ray attenuation information in the form of grayscale values and particularly for the coarser pyrite (Fig. 9). All grains labelled either pyrite (and subtypes of pyrite) or gold were used as input for machine learning algorithms. Grain characteristics (e.g., sphericity, X-ray attenuation values, volume) were used as machine learning features. Feature selection was performed to determine the best combination of features (Hastie et al., 2009). Using these features, it is possible to identify critical differences between gold–pyrite–uraninite and other ore constituents and leverage these relationships for inference. In this manner, μCT data are readily usable for the discrimination of the desirability of gold grains. This is a supervised machine learning task, for which there are many algorithms available. In this study, we did not perform an exhaustive comparison of all machine learning algorithms but rather demonstrate the feasibility of this approach using the support vector machine (SVM) algorithm (Cristianini & Ricci, 2008).

Inspection of Figure 9 indicates that μCT gray values (which were mapped to a range of attenuation coefficients per sample) can be used to discriminate gold from gangue minerals such as pyrite. Using these features (Figure 10), we trained an SVM, and the algorithm's performance was assessed. Results showed that the F1 and accuracy scores using the trained SVM to perform a fivefold cross-validation, randomized and shuffled 100 times over the entire database was exactly 1.00 for the discrimination between pyrite and gold, and between

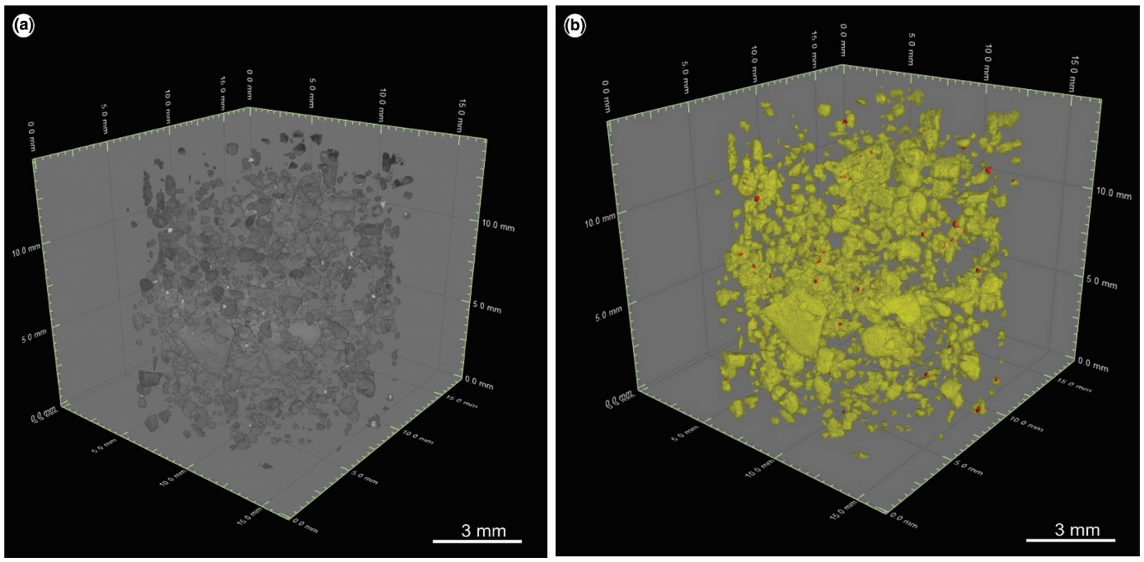

Figure 9. Automated classification of gold using the support vector machine (SVM) algorithm. (**a**) 16-bit grayscale image (X-ray attenuation quantized to roughly 65,000 shades of gray) with sparse gold appearing bright white against darker gray pyrite grains. Note that the occasional darkening of gray pyrite is an artefact to simulate shading for 3D visualization. (**b**) Artificial color segmentation to better visualize pyrite (yellow) and gold (red).

various types of pyrite. However, because gray values (and therefore X-ray attenuation) were used as features, it is unclear whether different types of pyrite can be distinguished if they are within the same sample volume, unless they are substantially different compositionally (e.g., they are likely to be mapped to similar gray values). We attempted to discriminate between pyrite and gold, as well as between various types of pyrite using solely physical characteristics of minerals (projected area along the xy-, xz- and yz-planes [mm^2], surface [mm^2], gap [mm] and sphericity). However, this was unsuccessful, because it was impossible to distinguish between pyrite and gold using these features and while it was possible to distinguish between the various types of pyrite, the F1 and accuracy scores were low (0.51 and 0.61, respectively). Therefore, the prediction of mineral composition is far more practical than the discrimination of pyrite and gold using grain morphology for similar types of μCT data. However, the ability to rapidly assess sample mineral composition is useful for assaying and geometallurgy. Other types of μCT data that describe other physical characteristics of particles, as well as raw images of particles may offer more useful characteristics for the differentiation of subtypes of minerals.

DISCUSSION

Geometry and Extent of the Black Reef Formation

Seismic data enhanced by seismic attributes show clear stratigraphic continuity and shallow dip (< 10°) of the Black Reef Formation (Figs. 3 and 4). The shallow dip of the Black Reef Formation is substantially different compared to the older gold-bearing horizons of the Ventersdorp and Witwatersrand Supergroups (Fig. 4). Localized dip variations were linked to structural interferences, especially major faults and dikes that cut across the Black Reef Formation and older volcano-sedimentary successions. Compared to most Witwatersrand Supergroup gold-bearing horizons, the Black Reef Formation seems to have been affected by post-depositional fracturing and faulting (Fig. 11). The Black Reef Formation's lithological composition and geological setting are identical to those in, and thus considered to be the result of, rift-type tectonic settings formed by stretching or thinning the continental lithosphere (Allen et al., 2015). Such rift-type basins were common during the Meso- to Neoarchean and these have been documented extensively by Kinsman (1975) and Veevers (1981). In the early stages of

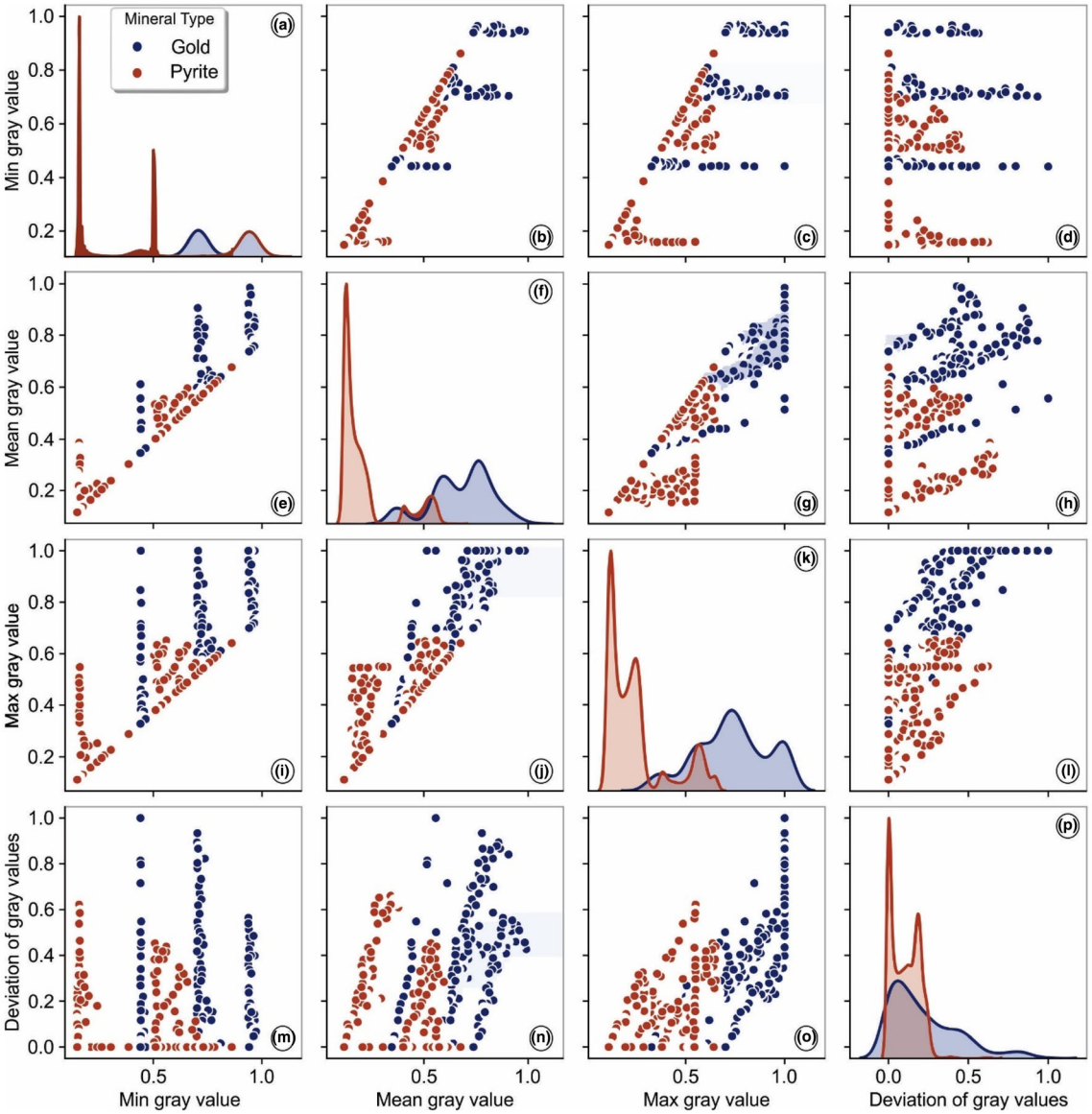

Figure 10. Scatter correlation matrix of machine learning input parameters obtained from 3D µCT (n = 19,620). The kernel density estimates (a, f, k and p) depict how each µCT numeric variable is distributed using a Gaussian kernel density estimation (the bandwidth is determined using the rule of Scott (1992)).

forming Archean and Paleoproterozoic rift-type basins, intra-continental sags (cratonic basins) and continental rim basins are present, lacking brittle stretching but containing extensional fault systems with influences related to topography. This interpretation seems plausible based on the distribution of faults in the Black Reef Formation, especially those within its gold-bearing horizon.

Older faults affecting the Black Reef Formation generally showed displacements of > 50 m, while younger faults formed during the thermal sag phase are limited to the Black Reef Formation and have displacements of < 50 m. The most common feature observed from the 3D seismics was the undulation of the Black Reef Formation, likely related to the paleotopographic surface on which the Black Reef Formation was deposited. The results derived from the interpreted 3D seismic data constrain the structural pattern and geometry of the Black Reef orebody (Fig. 11).

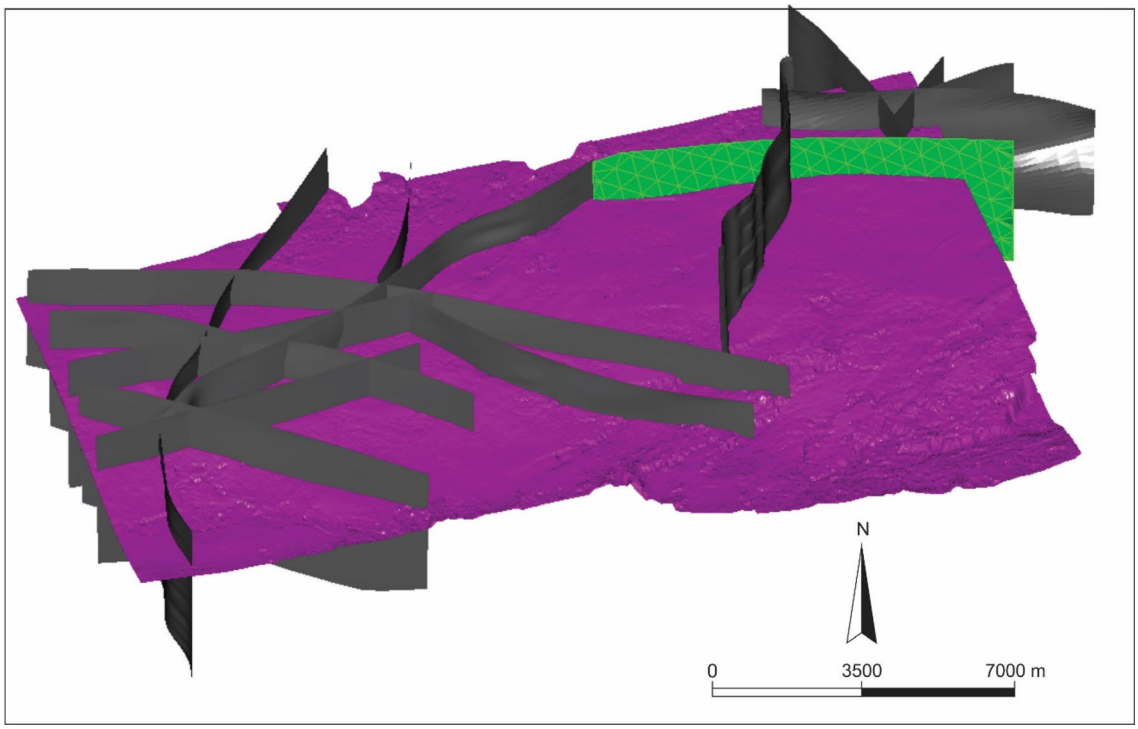

Figure 11. Model of the gold-bearing Black Reef Formation horizon and geological structures in the study area. Gray = faults, green = dike, and purple = Black Reef Formation horizon.

Prevention of Hazards Using Deposit-Scale Structural Models

One of the most significant uncertainties in underground operations is the potential for a mine to encounter unexpected geological structures such as faults and dikes (Stevenson et al., 2003; Fig. 11). The presence of faults, in particular, has several detrimental effects on underground mining. They may cause (a) physical displacement of the reef horizon, which may make mining impractical, (b) loss of stability in hanging wall, and (c) migration of water and methane gas into underground workings. This study was able to effectively delineate major and small-scale faults in the seismic data using seismic attributes to determine their dips, orientation, and throws.

Individual faults were digitized to determine their dips and strikes, from which 3D point clouds were produced. Initially, a linear or quadratic polynomial surface was fitted to each cloud, which was satisfactory if a fault was near-planar but performed poorly if the fault shape was more complex (which is the case for majority of the faults in our study area). Therefore, each fault was modeled with multiple planes, and the median value was used to characterize the fault. Once the median surface was established, each sub-fault's dip and dip direction was calculated. In general, the data showed that the faults could be classified easily into different strike- and dip-specific classes. The strike classes were (1) 0–30°, (2) 30–70°, (3) 70–100°, (4) 100–140°, and (5) 140–180°. The dip classes were (1) 20–40°, (2) 40–60, and (3) 60–90°. A major consideration in orebody/horizon modeling is fault geometric attributes, especially dip. It was considered more unstable to have the hanging wall of an orebody/horizon block bound by shallow-dipping (0– 45°) faults than blocks bound by steeply dipping (60–80°) faults.

Integration of Machine Learning for Mineral Classification

The ability to assess 3D mineral texture rapidly and classify minerals automatically has enormous potential in the mineral extraction and processing industry (Hanna & Ketcham, 2017). Many tasks in

the resource extraction and processing cycle are either critical or are becoming critical to the industry's success. These include resource estimation and modeling, material pre-concentration and sorting; leveraging geometallurgy to optimize extraction and processing; and automation (Lishchuk et al., 2020; Nwaila et al., 2020c). In all these tasks, leveraging online sensors, data and machine learning will become a critical differentiator between resource extraction success and failure in the era of digitization. During the resource estimation and modeling process, an accurate resource model is becoming increasingly important to mitigate against the deleterious effects of low-grade, high variability, and less desirable ores.

To increase the accuracy of resource models, it is crucial to increase sampling density and operational feedback in the form of rapid in situ assessment to fine-tune the models during operation. Without online sensors, data and machine learning, this is a difficult task as the turnaround time for sampling and assaying samples after a stope has been made available for extraction can be prolonged (up to 14 days) and vastly increasing sample density is not financially desirable. Instead, a modern approach should focus on a large reduction in cost per sample analyzed and in a manner that can be rapidly performed, such as with μCT-based analytical methods. For grade estimation, the μCT assays need not reach the level of accuracy of chemical assays, as substantially more data can be generated with minimal cost (da Costa et al., 2022). In this manner, resource models can be more granular and at a quantization that is directly utilizable by extraction. This creates higher-resolution models that, at the block level, may exceed the capabilities of those derived from the comparatively sparser-sampled traditional resource estimation approach by gaining spatial resolution at the expense of per-sample analytical accuracy (Lishchuk et al., 2019).

Material pre-concentration and sorting are important, probably critically so with low-grade ores and secondary metallurgical streams. In all cases, the ability to concentrate the resource rapidly for processing preparation increases the financial viability of resources that may otherwise be financially unviable for extraction. The material characterization information derived from the online sensors, such as X-ray spectrometers can be leveraged to understand the geometallurgy of a stream of incoming material to the processing plant. Such information is highly valuable for the processing plant to optimize its processing parameters by acting on the characteristics of resource-bearing material that can be derived from the pre-concentration stage (Jardine et al., 2018; Guntoro et al., 2019a, 2019b). This allows more selective and higher efficiency processing methods that maximize processing efficiency. Because these tasks all rely on sensors, data and machine learning, they can all be partially or wholly automated to improve throughput, efficiency and financial viability.

Importance of Relationship Between Gold and Pyrite

Gold deportment in the mineable reserve can firmly control final recovery. This highlights the rise of the modern geometallurgical approach to mineral processing and plant flowsheet design. While gold tends to form metallic grains in nature, a large proportion could be enclosed in durable host minerals such as quartz and pyrite or soft and easily smeared hydrocarbons, such as pyrobitumen. Therefore, the successful liberation of tiny particle sizes is a key factor in any recovery strategy, especially where the grades are marginally profitable. The auriferous conglomerate samples of the Black Reef Formation contain substantial pyrite-hosted gold. The relationship between gold and pyrite in the Witwatersrand-type gold deposits provides a qualitative assessment of gold association and liberation characteristics (Fig. 12). Not all pyrite grains in the Witwatersrand-type gold deposits are associated with gold. When compared to other pyrite grains, previous studies have shown that detrital pyrite grains have high trace element contents, including very high gold contents (Agangi et al., 2015). However, for the gold-bearing Black Reef Formation, hydrothermal pyrite is also associated with gold (Fuchs et al., 2016). Distinguishing between gold and pyrite, as well as between various types of pyrite, may be feasible in many cases using μCT data and machine learning. Gold in the Black Reef Formation was introduced via multiple processes, including: (a) recycling of gold-rich Witwatersrand lithologies (or reefs) in the underlying

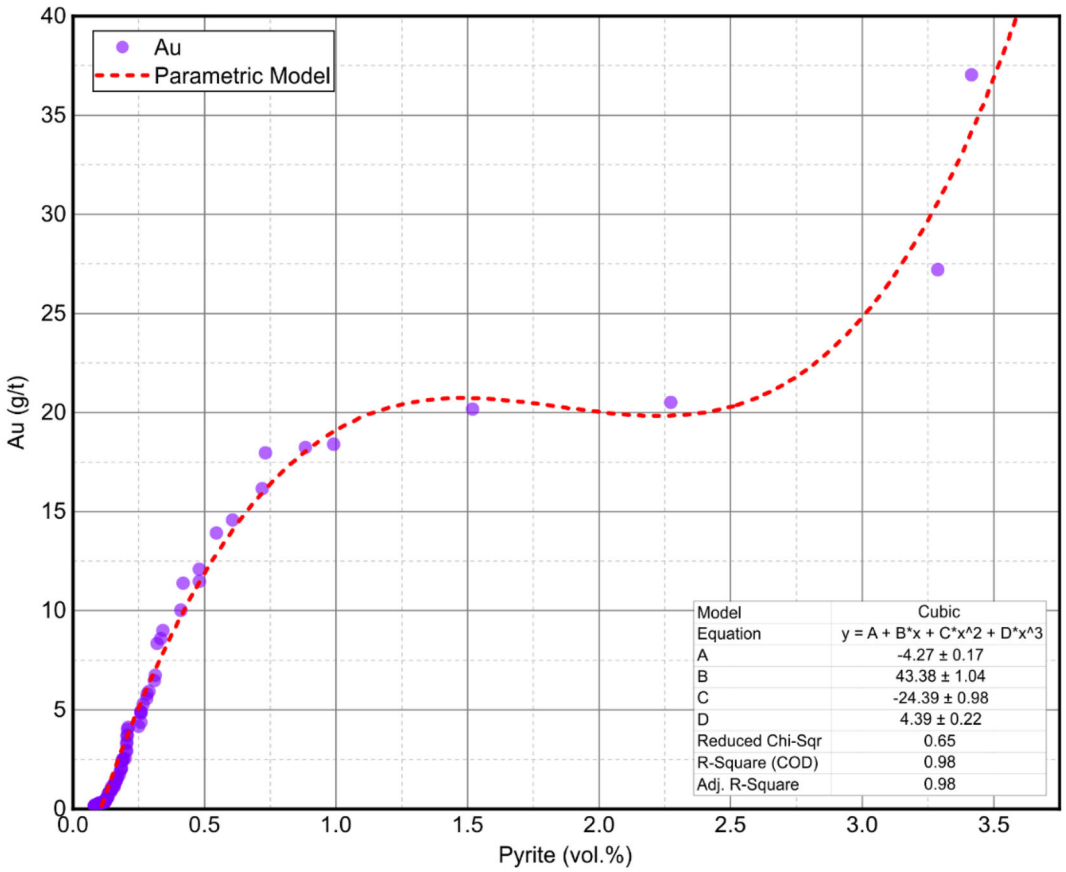

Figure 12. Modeling the relationship between pyrite and gold using outputs from μCT. Dataset is presented in Supplementary Data S1.

strata which means that gold could have been incorporated during pyrite abrasion or adsorbed during diagenesis (Nwaila et al., 2020a); and (b) reworking during successive stages of the Bushveld Igneous Complex magmatism and the Vredefort meteorite impact (Frimmel, 2014; Fuchs et al., 2016; Frimmel & Nwaila, 2020). Meteorite-induced seismic activity likely led to the reactivation of dormant faults, clearly imaged in the seismic data (Fig. 11; Manzi et al., 2013; Nwaila et al., 2020a). Movement along faults inevitably resulted in the creation of numerous microfractures. Fault movement and microfractures promoted concomitant fluid infiltration and circulation. This also explains the association of gold in various pyrite generations in the Black Reef Formation and associated ore constituents, crack-filled gold in quartz and pyrobitumen. The lithological, sedimentological and mineralogical characteristics indicate that the gold-enriched Black Reef Formation is a member of the Witwatersrand-type deposit class.

Implication for Mineral Processing

Modeling of the Black Reef Formation horizon and structural features (Figs. 3, 4, 11), mineral grain size distributions (Fig. 8), and prediction of the spatial distribution of gold using sparse data from drill holes and underground samples can be considered groundwork for more efficient mining and mineral processing stages. Geometallurgy is a multidisciplinary approach that establishes a spatial prediction model for production management by connecting the three main pillars of the mining value chain: (1) geology and geophysics; (2) mining methods; and (3) mineral processing and extractive metallurgy. The purpose of a geometallurgical

model is to provide a quantitative prediction of metallurgical performance, i.e., concentration quality, recovery rate, throughput, environmental impacts, and overall economic fluctuations (Ghorbani et al., 2013a, 2013b; Hilden and Powell, 2017; Koch et al., 2019; Guntoro et al., 2020, 2021). While the concept is not new, recent advancements in geophysical approaches, chemical characterization methods, automated mineralogy (in 2D and 3D), data processing, and metallurgical testing have made it more practical in practice. This has resulted in a new characterization workflow that includes multiscale (e.g., meso-, micro- or nanoscale) characterization techniques (da Costa et al., 2022). With the rapid advancement of ore characterization tools and techniques in the 2D and 3D environments, such as X-ray fluorescence computed tomography for quantitative chemical, mineralogical and textural characterization of ores (Chen et al., 2020), it is of utmost necessity to move toward dry laboratories (data-centric and computation-heavy laboratories) and modernized data management practices. This type of environment will provide the ideal technology and expertise to analyze both old and new data to extract multi-timescale information. Short-term information can be utilized to provide just-in-time feedback to existing processing plants, while long-term knowledge can guide the design and refinement of new mineral processing and extractive metallurgy units (see Ghorbani et al., 2020 for a detailed discussion).

CONCLUSIONS

Deposit-scale geophysical and geological models can help minimize uncertainty in a mineral deposit. At the same time, rapid reporting of mineral textures and distributions can help with the decision-making process on prioritization of minable blocks/horizons and prediction of ore variability at the metallurgical plant. This can be best addressed by utilizing 3D reflection seismic data enhanced by seismic attributes, geological modeling, and the use of cost-effective machine learning workflows, some of which may even rely on legacy-types of data. Deposit-scale modeling using seismic reflection data to map structures that control the gold-bearing Black Reef Formation combined with 3D μCT to determine ore grades rapidly and accurately are steps that could help bridge the existing gap between exploration in-mine geological modeling and uncertainty quantification. The use of larger-scaled models, such as those resulting from seismic imaging and geological modeling, and the use of higher resolution resource models, such as those resulting from μCT-based assays form a formidable framework that may well enable more efficient and sustainable resource extraction. Where applied, such a framework would likely improve our understanding of orebody geometry, uncertainty in modeling, safety in mining, and the development of efficient methods for metallurgical treatment of ores. These framework components are transitional toward a fully digitized mining environment, where online sensor networks would generate modernized data streams. Future research that could assist with adaptation of the proposed framework in the mining industry could include:

1. Integrating geophysical and geological data as a routine workflow for implicit modeling and mine planning.
2. Investigation and comparison between deposit-scale geological structures and mining-induced seismic activity on a mine scale.
3. Further research in various geological settings using methods outlined in this paper to provide guidance and improve workflows on quantitative uncertainty assessments of model interpretations.

ACKNOWLEDGMENTS

Critiques by two anonymous reviewers greatly improved the development of the final manuscript. The authors thank Leon Tolmay for his guidance on the block modeling process. We also thank Jason Kirk (University of Arizona) for his help with pyrite separation and classification. The authors thank Prof. E. J. M. (John) Carranza for editorial handling.

FUNDING

This study was supported by a Department of Science and Innovation (DSI)-National Research Foundation (NRF) Thuthuka Grant (Grant UID: 121973) and DSI-NRF CIMERA.

DECLARATIONS

Conflict of Interest The authors declare that they have no known competing financial interests of personal relationships that could have appeared to influence the work reported in this paper.

SUPPLEMENTARY INFORMATION

The online version contains supplementary material available at https://doi.org/10.1007/s11053-022-10064-5.

SUPPLEMENTARY INFORMATION

The online version contains supplementary material available at https://doi.org/10.1007/s11053-022-10064-5.

REFERENCES

Agangi, A., Hofmann, A., Rollion-bard, C., Marin-Carbonne, J., Cavalazzi, B., Large, R., & Meffre, S. (2015). Gold accumulation in the Archaean Witwatersrand Basin, South Africa: Evidence from concentrically laminated pyrite. *Earth Science Reviews, 140*, 27–53.

Allen, P., Eriksson, P., Alkmim, F., Betts, P., Catuneanu, O., Mazumder, R., Meng, Q., & Young, G. M. (2015). Classification of basins, with special reference to Proterozoic examples. In R. Mazumder, & P. Eriksson (Eds.), *Precambrian basins of India: stratigraphic and tectonic contexts* (pp. 5–28). Geological Society, London. doi:https://doi.org/10.1144/M43.2.

Antrobus, E. S. A., Brink, W. C. J., Brink, M. C., Caulkin, J., Hutchinson, R. I., Thomas, D. E., van Graan, J. A., & Viljoen, J. J. (1986). The Klerksdorp Goldfield. In C. R. Anhaeusser & S. Maske (Eds.), *Mineral deposits of southern Africa* (pp. 549–598). Geological Society of South Africa.

Bam, L. C., Miller, J. A., & Becker, M. (2020). A mineral X-ray linear attenuation coefficient tool (MXLAC) to assess mineralogical differentiation for X-ray computed tomography scanning. *Minerals, 10*(5), 441.

Barton, E. S., & Hallbauer, D. K. (1996). Trace element and U-Pb isotope compositions of pyrite types in the Proterozoic Black Reef, Transvaal Sequence, South Africa: Implication in genesis and age. *Chemical Geology, 133*, 173–199.

Button, A. (1973). A regional study of the stratigraphy and development of the Transvaal Basin in the eastern and northeastern Transvaal. PhD thesis, University of the Witwatersrand, Johannesburg, pp. 352.

Chen, Z., Zhang, S., & Li, L. (2020). Experimental demonstration of X-Ray Fluorescence CT using a spatially distributed multibeam X-Ray source. *Frontiers in Physics, 8*, 462.

Cristianini, N., & Ricci, E. (2008). Support vector machines. In M.Y. Kao (Ed.), *Encyclopaedia of Algorithms*. Springer, New York. doi:https://doi.org/10.1007/978-0-387-30162-4_415.

da Costa, G., Hofmann, A., & Agangi, A. (2020). A revised classification scheme of pyrite in the Witwatersrand Basin and application to placer gold deposits. *Earth Science Reviews, 201*, 103064.

da Costa, M. F., Kyle, J. R., Lobato, L. M., Ketcham, R. A., Figueiredo, R. C., & e Silva, F., & Fernandes, R. C. (2022). Orogenic gold ores in three-dimensions: a case study of distinct mineralization styles at the world-class Cuiabá deposit, Brazil, using high-resolution X-ray computed tomography on gold particles. *Ore Geology Reviews, 140*, 104584.

Els, B. G., van den Berg, W. A., & Mayer, J. J. (1995). The Black Reef quartzite formation in the western Transvaal: Sedimentological and economic aspects, and significance for basin evolution. *Mineralium Deposita, 30*, 112–123.

Eriksson, P. G., Altermann, W., & Hartzer, F. J. (2006). The Transvaal Supergroup and its precursors. In M. R. Johnson (Ed.), *The Geology of South Africa* (pp. 237–260). Geological Society of South Africa.

Evans, C. L., Wightman, E. M., & Yuan, X. (2015). Quantifying mineral grain size distributions for process modelling using X-ray micro-tomography. *Minerals Engineering, 82*, 78–83.

Frimmel, H. E. (2014). A giant Mesoarchean crustal gold-enrichment episode: Possible causes and consequences for exploration. In K. D. Kelley, & H. C. Golden (Eds.), *Building Exploration capability for the 21st century* (vol. 18, pp. 209–234). Special publication of the Society of Economic Geologists. doi:https://doi.org/10.5382/SP.18.

Frimmel, H. E., & Nwaila, G. T. (2020). Geologic evidence of syngenetic gold in the Witwatersrand Goldfields, South Africa. In R. H. Sillitoe, R. J. Goldfarb, F. Robert, & S. F. Simmons (Eds.), *Geology of the major gold deposits and provinces of the world* (vol. 23, pp. 645–668). Special publication of the Society of Economic Geologists. doi:https://doi.org/10.5382/SP.23.31.

Frimmel, H. E. (2005). Archaean atmospheric evolution: Evidence from the Witwatersrand goldfields, South Africa. *Earth Science Reviews, 70*, 1–46.

Frimmel, H. E. (2019). The Witwatersrand Basin and its gold deposits. In A. Kroner & A. Hofmann (Eds.), *The Archean geology of the Kaapvaal Craton, Southern Africa* (pp. 325–345). Springer.

Fuchs, S. (2015). The role of hydrocarbons in the Witwatersrand gold and uranium deposits, and the genesis of Witwatersrand-style Black Reef deposits, South Africa. PhD thesis, McGill University, Montréal, pp. 191.

Fuchs, S., William-Jones, A. E., & Przybylowicz, W. J. (2016). The origin of gold and uranium ores of the Black Reef Formation, Transvaal Supergroup, South Africa. *Ore Geology Reviews, 72*(1), 149–164.

Gauert, C., Brauns, M., Batchelor, D. & Simon, R. (2011). Gold Provenance of the Black Reef Conglomerate, West and East Rand, South Africa. In *SGA biennial conference 2011* (vol. 2011/1).

Ghorbani, Y., Becker, M., Petersen, J., Mora, S. H., Mainza, A., & Franzidis, J.-P. (2011). Use of X-ray computed tomography to investigate the crack distribution and mineral dissemination in sphalerite ore particles. *Minerals Engineering, 24*(12), 1249–1257.

Ghorbani, Y., Becker, M., Petersen, J., Mainza, A. N., & Franzidis, J.-P. (2013a). Investigation of the effect of mineralogy as rate-limiting factors in large particle leaching. *Minerals Engineering, 52*, 38–51.

Ghorbani, Y., Petersen, J., Becker, M., Mainza, A. N., & Franzidis, J.-P. (2013b). Investigation and modelling of the progression of zinc leaching from large sphalerite ore particles. *Hydrometallurgy, 131–132*, 8–23.

Ghorbani, Y., Nwaila, G. T., Zhang, S. E., & Hay, M. P. (2020). Repurposing legacy metallurgical data Part I: a move toward

dry laboratories and data bank. *Minerals Engineering, 159*, 106646.
Guntoro, P. I., Ghorbani, Y., Butcher, A. R., Kuva, J., & Rosenkranz, J. (2020). Textural quantification and classification of drill cores for geometallurgy: Moving toward 3D with X-ray microcomputed tomography (μCT). *Natural Resources Research, 29*(6), 3547–3565.
Guntoro, P. I., Ghorbani, Y., Koch, P.-H., & Rosenkranz, J. (2019a). X-ray computed microtomography (μCT) for mineral characterisation: A review of data analysis methods. *Minerals, 9*(3), 183.
Guntoro, P. I., Tiu, G., Ghorbani, Y., Lund, C., & Rosenkranz, J. (2019b). Application of machine learning techniques in mineral phase segmentation for X-ray microcomputed tomography (μCT) data. *Minerals Engineering, 142*, 105882.
Guntoro, P. I., Ghorbani, Y., Parian, M., Butcher, A. R., Kuva, J., & Rosenkranz, J. (2021). Development and experimental validation of a texture-based 3D liberation model. *Minerals Engineering, 164*, 106828.
Guy, B. M., Ono, S., Gutzmer, J., Lin, Y., & Beukes, N. J. (2014). Sulphur sources of sedimentary ''buckshot'' pyrite in the auriferous conglomerates of the Mesoarchaean Witwatersrand and Ventersdorp Supergroups, Kaapvaal Craton, South Africa. *Mineralium Deposita, 49*, 751–775.
Hanna, R. D., & Ketcham, R. A. (2017). X-ray computed tomography of planetary materials: A primer and review of recent studies. *Chemie Der Erde, 77*(4), 547–572.
Hartnady, C. J. (2009). South Africa's gold reserves and production. *South African Journal of Sciences, 105*(9–10), 328–329.
Hastie, T., Tibshirani, R., & Friedman, J. (2009). Boosting and additive trees. In *The elements of statistical learning* (pp. 337–387). Springer, New York. doi:https://doi.org/10.1007/978-0-387-84858-7_10.
Henry, G., & Master, S. (2008). Black Reef project final report. *Council for Scientific and Industrial Research (CSIR) and University of the Witwatersrand*, Johannesburg, pp. 61.
Hilden, M. M., & Powell, M. S. (2017). A geometrical texture model for multi-mineral liberation prediction. *Minerals Engineering, 111*, 25–35.
Hoffman, J. W. (2012). Process description for micro-focus X-ray investigation of source at MIXRAD facility. *Necsa internal report,* RS-MFX-PRO-12002.
Hofmann, A., Bekker, A., Rouxel, O., Rumble, D., & Master, S. (2009). Multiple sulphur and iron isotope composition of detrital pyrite in Archaean sedimentary rocks: A new tool for provenance analysis. *Earth and Planetary Science Letters, 286*(3–4), 436–445.
Jardine, M. A., Miller, J. A., & Becker, M. (2018). Coupled X-ray computed tomography and grey level co-occurrence matrices as a method for quantification of mineralogy and texture in 3D. *Computers and Geosciences, 111*, 105–117.
Ketcham, R. A. (2005). Computational methods for quantitative analysis of three-dimensional features in geological specimens. *Geosphere, 1*(1), 32–41.
Ketcham, R. A., & Hildebrandt, J. (2014). Characterizing, measuring, and utilizing the resolution of CT imagery for improved quantification of fine-scale features. *Nuclear Instruments and Methods in Physics Research Section b: Beam Interactions with Materials and Atoms, 324*, 80–87.
Ketcham, R. A., & Mote, A. S. (2019). Accurate measurement of small features in X-ray CT data volumes, demonstrated using gold grains. *Journal of Geophysics Research: Solid Earth, 124*(4), 3508–3529.
Kinsman, D. J. J. (1975). Rift valley basins and sedimentary history of trailing continental margins. In A. G. Fischer & S. Judson (Eds.), *Petroleum and Global Tectonics* (pp. 83–126). Princeton University Press.
Koch, P.-H.H., Lund, C., & Rosenkranz, J. (2019). Automated drill core mineralogical characterisation method for texture classification and modal mineralogy estimation for geometallurgy. *Minerals Engineering, 136*, 99–109.
Kyle, J. R., & Ketcham, R. A. (2015). Application of high resolution X-ray computed tomography to mineral deposit origin, evaluation, and processing. *Ore Geology Reviews, 65*(4), 821–839.
Kyle, J. R., Mote, A. S., & Ketcham, R. A. (2008). High resolution X-ray computed tomography studies of Grasberg porphyry Cu–Au ores, Papua, Indonesia. *Mineralium Deposita, 43*, 519–532.
Lishchuk, V., Koch, P.-H., Ghorbani, Y., & Butcherc, A. R. (2020). Towards integrated geometallurgical approach: critical review of current practices and future trends. *Minerals Engineering, 145*, 106072.
Lishchuk, V., Lund, C., & Ghorbani, Y. (2019). Evaluation and comparison of different machine-learning methods to integrate sparse process data into a spatial model in geometallurgy. *Minerals Engineering, 134*, 156–165.
Manzi, M. S. D., Durrheim, R. J., Hein, K. A. A., & King, N. (2012a). 3D edge detection seismic attributes used to map potential conduits for water and methane in deep gold mines in the Witwatersrand Basin, South Africa. *Geophysics, 77*, 133–147.
Manzi, M. S. D., Gibson, M. A. S., Hein, K. A. A., King, N., & Durrheim, R. J. (2012b). Application of 3D seismic techniques to evaluate ore resources in the West Wits Line goldfield and portions of the West Rand goldfield, South Africa. *Geophysics, 77*(5), 163–171.
Manzi, M. S. D., Hein, K. A. A., Durrheim, R. J., & King, N. (2014). The Ventersdorp Contact Reef model in the Kloof Gold Mine as derived from 3D seismics, geological mapping and exploration borehole datasets. *International Journal of Rock Mechanics and Mining Sciences, 66*, 97–113.
Manzi, M. S. D., Hein, K. A. A., King, N., & Durrheim, R. J. (2013). Neoarchaean tectonic history of the Witwatersrand Basin and Ventersdorp Supergroup: New constraints from high resolution 3D seismic reflection data. *Tectonophysics, 590*, 94–105.
McLoughlin, A. C. (2014). Geometallurgical examination of gold, uranium and thorium in the Black Reef Quartzite formation, Gold One International LTD, Springs. MSc thesis, University of Johannesburg, South Africa.
Minnitt, R. C. A. (2014). Sampling in the South African minerals industry. *Journal South African Institute of Mining and Metallurgy, 114*(1), 63–81.
Nwaila, G. T., Durrheim, R. J., Jolayemi, O. O., & Maselela, H. K. (2020a). Significance of granite-greenstone terranes in the formation of Witwatersrand-type gold mineralization: a case study of the Neoarchaean Black Reef Formation. *South Africa. Ore Geology Reviews, 121*, 103572.
Nwaila, G. T., Ghorbani, Y., Becker, M., Frimmel, H. E., Petersen, J., & Zhang, S. (2020b). Geometallurgical approach for implications of ore blending on cyanide leaching and adsorption behaviour of Witwatersrand gold ores, South Africa. *Natural Resources Research, 29*, 1007–1030.
Nwaila, G. T., Zhang, S. E., Frimmel, H. E., & Manzi, M. S. D. (2020c). Local and target exploration of conglomerate-hosted gold deposits using machine learning algorithms: A case study of the Witwatersrand gold ores, South Africa. *Natural Resources Research, 29*, 135–159.
Penning, W. H. (1891). A contribution to the geology of the Southern Transvaal. *Quarterly Journal of the Geological Society of London, 47*, 451.
Robb, L. J., Robb, V. M. (1998). Gold in the Witwatersrand Basin. In M. G. C. Wilson, & C. R. Anhaeusser (Eds.), *The mineral resources of South Africa* (pp. 294–349). Council for Geoscience, Pretoria, Handbook 16.
Sayab, M., Suuronen, J.-P., Hölttä, P., Aerden, D., Lahtinen, R., & Kallonen, A. K. (2016). High resolution X-ray computed

microtomography: A holistic approach to metamorphic fabric analyses. *Geology, 43*, 55–58.

Scott, D. W. (1992). *Multivariate density estimation: Theory, practice, and visualization*. Wiley.

Stevenson, F., Higgs, R. M. A., & Durrheim, R. J. (2003). Seismic imaging of precious and base-metal deposits in Southern Africa. In D. Eaton, B. Milkereit, & M. H. Salisbury (Eds.), *Hardrock Seismic Exploration* (pp. 141–156). Society of Exploration Geophysicists.

USGS (2021). Gold statistics and information, 2021 Annual Publication. US Geological Survey. https://www.usgs.gov/centers/national-minerals-information-center/gold-statistics-and-information.

Veevers, J. J. (1981). Morphotectonics of rifted continental margins in embryo (East Africa), youth (Africa-Arabia), and maturity (Australia). *Journal of Geology, 89*, 57–82.

Warlo, M., Bark, G., Wanhainen, C., Butcher, A., Forsberg, F., Lycksam, H., & Jukka, K. (2021). Multi-scale X-ray computed tomography analysis to aid automated mineralogy in ore geology research. *Frontiers of Earth Sciences, 9*, 789372.

Williams, C. A. (2020). Simplifying sample processing: new gold assay method offers faster turnaround. Canadian mining journal. https://www.canadianminingjournal.com/features/simplifying-sample-processing-new-gold-assay-method-offers-faster-turnaround/.

Withers, P. J., Bouman, C., Carmignato, S., Cnudde, V., Grimaldi, D., Hagen, C. K., Maire, E., Manley, M., Du Plessis, A., & Stock, S. R. (2021). X-ray computed tomography. *Nature Reviews Methods Primers, 1*, 18. https://doi.org/10.1038/s43586-021-00015-4.

Zeh, A., Wilson, A. H., & Gerdes, A. (2020). Zircon U-Pb-Hf isotope systematics of transvaal supergroup: constraints for the geodynamic evolution of the Kaapvaal Craton and its hinterland between 2.65 and 2.06 Ga. *Precambrian Research, 345*, 105760.

Zhang, S. E., Nwaila, G. T., Frimmel, H. E., Tolmay, L., & Bourdeau, J. E. (2021). Integration of machine-learning algorithms with Gompertz curves and kriging to estimate resources in gold deposits. *Natural Resources Research, 30*, 39–56.